Hyperfine Interact
DOI 10.1007/s10751-013-0926-2

Controlled crystallization a ionic conductivity of nanostructured $LiNbFePO_4$ glass ceramic

M. Y. Hassaan · S. M Salem · M. G. Moustafa · S. Kubuki · K. Matsuda · T. Nishida

Abstract Glass sample with a composition of $Li_{1.3}Nb_{0.3}Fe_{1.7}(PO_4)_3$, prepared by a conventional melt-quenching method, was heat treated to obtain glass ceramics of NASICON type. Glass transition (T_g) and crystallization (T_c) temperatures of as-quenched glass sample were determined by differential thermal analysis (DTA). X-ray diffraction (XRD) patterns also confirmed the formation of glass sample. After heat treatment above T_c, precipitation of crystalline particles with NASICON-type structure was confirmed by XRD. Valency and local structure of Fe atoms were investigated by Mössbauer spectroscopy at room temperature. DC-conductivity and impedance measurements of the glass ceramics proved the increased electrical conduction caused by heat treatment.

Keywords NASICON-type glass ceramic · $Li_3Fe_2(PO_4)_3$ · Ionic conductivity

Proceedings of the 32nd International Conference on the Applications of the Mössbauer Effect (ICAME 2013) held in Opatija, Croatia, 1–6 September 2013.

M. Y. Hassaan (✉) · S. M. Salem · M. G. Moustafa
Department of Physics, Faculty of Science, Al-Azhar University,
Nasr City 11884, Cairo, Egypt
e-mail: myhassaan@yahoo.com

S. Kubuki · K. Matsuda
Department of Chemistry, Graduate School of Science and Engineering,
Tokyo Metropolitan University, Minami-Osawa 1-1,
Hachi-Oji, Tokyo 192-0397, Japan

T. Nishida
Department of Biological and Environmental Chemistry,
Faculty of Humanity-Oriented Science and Engineering,
Kinki University, Iizuka 820-8555, Japan

Published online: 25 October 2013

1 Introduction

Much attention has been paid to alternative energy technologies, which require suitable materials having high lithium-ion conductivity. In this context, there is considerable interest in NASICON-type compounds having a general formula of $AM_2(PO_4)_3$ (A: alkali ion, M: one or more ions of tri-, tetra- or penta-valent states), which offer high ionic conductivity, high thermal stability, low thermal conductivity and low thermal expansion [1, 2]. Crystallographic NASICON structure was first identified by Hagman and Kierkegaard [3]; representative structure is rhombohedral with space group *R*3'c. Some compounds, however, have a low temperature phase of monoclinic symmetry [4–6]. The framework is built up of $M_2(PO_4)_3$ units in which two MO_6 octahedra and three PO_4 tetrahedra share oxygen atoms. They form conducting channels and two types of interstitial spaces where conducting cations are distributed. Structural and electrical properties of NASICON-type compounds are known to vary with the composition of the framework.

In the present work, we investigated glass sample with a composition of $Li_{1.3}Nb_{0.3}Fe_{1.7}(PO_4)_3$ and its related glass ceramics. Local structure of these samples were investigated by means of FT-IR and ^{57}Fe Mössbauer spectroscopy.

2 Experimental

$Li_{1.3}Nb_{0.3}Fe_{1.7}(PO_4)_3$ glass was prepared by conventional melt-quenching technique with analytical reagent grade of chemicals. After being pulverized in an agate mortar, the reagent mixture was calcined with an alumina crucible in an electric furnace at 300 °C for 2 h and at 600 °C for 4 h, in order to decompose the Li_2CO_3 and $NH_4H_2PO_4$ completely. After having been cooled to room temperature in air, the mixture was ground well, and was melted at 1200 °C for 1 h in an electric furnace, in order to increase the homogeneity of the glass sample. The melt was poured as quickly as possible on a copper plate at room temperature and was pressed with two copper plates, yielding a glass plate of about 1.5 mm thickness. Glass sample was kept in a desiccator to prevent it from absorbing moisture.

Glass ceramics were prepared by heating the glass plates by two-step heat treatments on the basis of the data obtained from DTA (Shimadzu). Heat treatment was first carried out for 2 h at a given temperature between glass transition temperature (T_g) and crystallization temperature (T_c) for nucleation. Each sample was heated up to the temperature above T_c for the sufficient crystal growth, which was performed for 12 to 30 h.

Bulk density was measured at room temperature by the Archimedes method with carbon tetrachloride as the immersing liquid (ρ: 1.593 gcm^{-3}). XRD measurement was conducted using Rigaku RINT 2100 with CuK_α radiations (λ: 0.1541 nm). FT-IR spectra were recorded for all samples in the range of 400–4000 cm^{-1} using computerized FT-IR spectrophotometer: JASCO (FT-IR-300E) by KBr disk method.

DC electrical conductivity of glass and glass ceramics was measured by means of two-probe method, which is generally applied to those of which resistivity is more than 10 MΩ. Silver paste coated on the polished surface of each sample was attached to two copper lead wires used for electrodes. *Picometer-760* was used to collect the DC data over the temperature range of 300–600 K. Sample temperature

was measured by a chromel-alumel type K-thermocouple which was placed close to the sample. Complex impedance measurement was carried out in the frequency ranging from 42 Hz to 5 MHz at 300 K using HIOKI 1.03 LCR meter. Mössbauer spectra were measured in a standard transmission geometry, using a source of ^{57}Co (925 MBq) diffused in a rhodium matrix. Calibration of the spectrometer was made with a natural iron foil, which was also used as reference of isomer shift (δ).

3 Results and discussion

3.1 DTA

DTA curve for as-prepared $Li_{1.3}Nb_{0.3}Fe_{1.7}(PO_4)_3$ glass is shown in Fig. 1, which reflects glassy nature of the sample. DTA chart exhibits two endothermic minima which represent glass transition temperatures of T_{g1}, T_{g2} at around 435 and 565 °C, respectively, and successive exothermic peak corresponding to crystallization peak temperature (T_c) at around 676 °C, followed by two endothermic peaks due to re-melting temperatures of T_{m1} and T_{m2} at around 890 and 982 °C, respectively. Estimated T_g and T_c values are comparable to those reported for related sample having similar composition [7].

3.2 X-ray diffraction (XRD)

Figure 2 shows XRD patterns of $Li_{1.3}Nb_{0.3}Fe_{1.7}(PO_4)_3$ glass and glass ceramics. In the case of as-quenched sample, only halo peak was observed at around $2\theta = 25$ degrees.

After heat treatment, several sharp peaks were observed which were ascribed to $LiFe(P_2O_7)$ (JCPDS card 80-1371) having a structure similar to that of monoclinic $Li_3Fe_2(PO_4)_3$ crystals (JCPDS card 78-1106). Size of crystallite particle was calculated with a Williamson–Hall (W-H) plot [9] of $\beta \cos\theta$ against $\sin\theta$, expressed by:

$$\beta \cos\theta = \frac{c\lambda}{D} + 4\varepsilon \sin\theta \tag{1}$$

where β is the full-width at half maximum (FWHM), θ the Bragg angle, c the correction factor ($c \approx 1$), D the crystallite size, λ the wavelength of X-rays and ε the lattice strain. It is observed that the crystallite size was increased from 82 to 124 nm by increasing the heat treatment time, as given in Fig. 3.

3.3 Fourier-transform infrared spectroscopy

FT-IR spectroscopy is effective for the characterization of glass and glass ceramics. FT-IR absorption spectra of $Li_{1.3}Nb_{0.3}Fe_{1.7}(PO_4)_3$ system are shown in Fig. 4. In the case of as-quenched glass sample, the broad band observed at about 540 cm^{-1} is assigned to asymmetric bending mode of O–P–O units [10, 11]. After heat treatment this broad band was split into three bands as observed at 548, 574 and 611 cm^{-1}. Two bands at 548 and 574 cm^{-1} are assigned to asymmetric bending vibration modes of O–P–O units [10, 11], while the band at 611 cm^{-1} to harmonic bending vibration of O–P–O [11, 12]. This band might be ascribed to the vibrational coupling of (Nb–O)

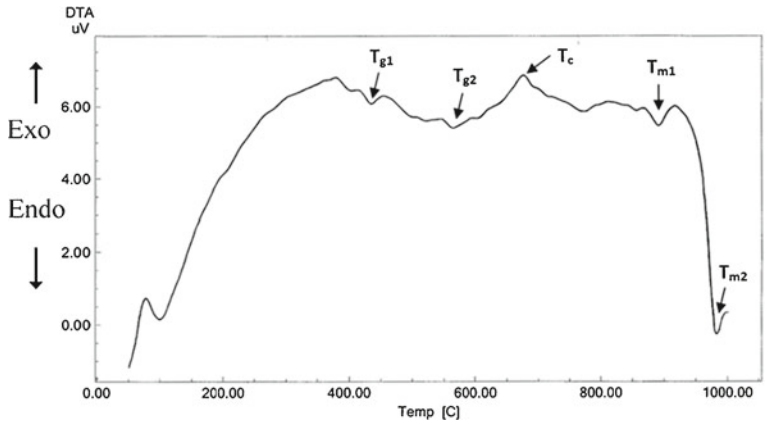

Fig. 1 DTA Curve of $Li_{1.3}Nb_{0.3}Fe_{1.7}(PO_4)_3$ glass

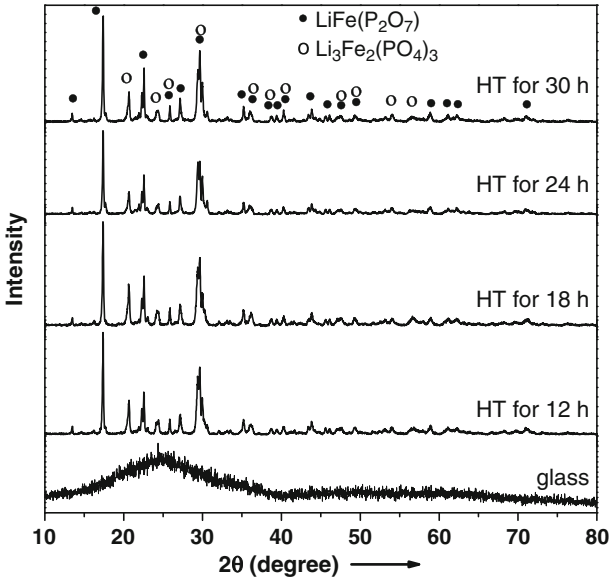

Fig. 2 XRD patterns of glass and glass-ceramics prepared by heat treatment (HT)

and (O–P–O) stretching modes with deformation [13]. A shoulder peak observed at 760 cm^{-1} in as-quenched glass is attributed to symmetric stretching vibration of P–O–P bridging bonds of pyrophosphate $(P_2O_7)^{4-}$ units [14]. This peak was also observed after heat treatment for different times. The absorption bands in the region of 925–949 cm^{-1} reflect ionic $(PO_4)^{3-}$ group vibration [11, 15]. Generally, the vibrational modes of NASICON phases can be assigned to tetrahedral PO_4 units (internal and external modes) and to lattice modes of metal with octahedral symmetry. Since the bands corresponding to PO_4 unit are more intense than those of metal-octahedra, the presence of ionic $(PO_4)^{3-}$ groups indicates the formation of NASICON phase. The observed bands in the region 1070–1125 cm^{-1} may be due to the ionic

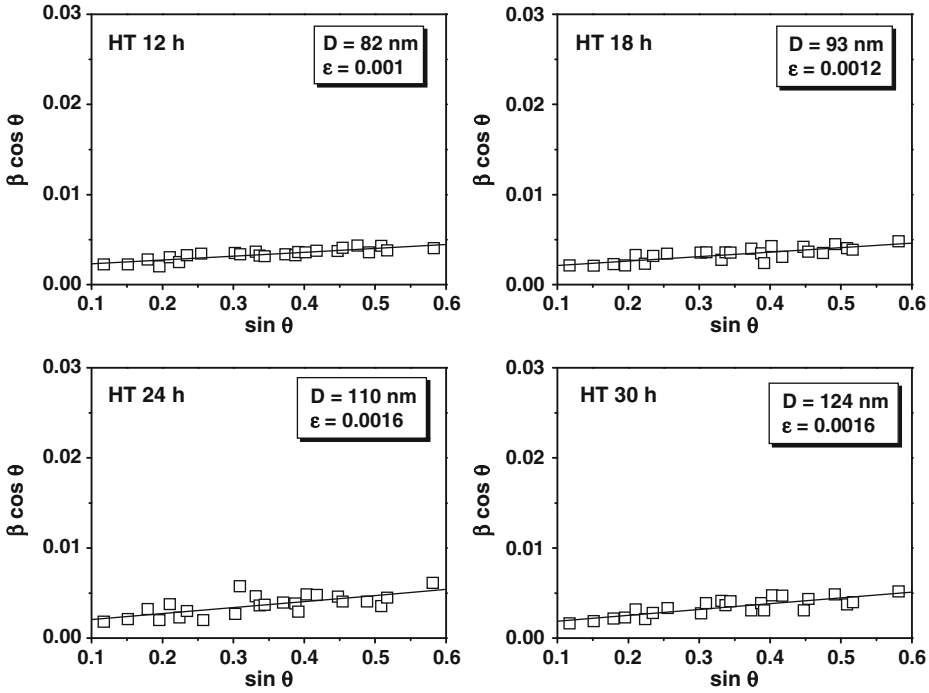

Fig. 3 W-H plot for glass ceramics

$(P–O)^{(-)}$ vibration [11, 16, 17]. The absorption band observed at 1620 cm^{-1} is associated with the deformational vibration mode of the H_2O [11, 18]. The bands in the region 3440–3453 cm^{-1} will be due to the stretching vibration mode of OH groups in water molecules [18].

3.4 Mössbauer spectroscopy

Mössbauer spectra measured at room temperature are shown in Fig. 5. Each spectrum was analyzed into one paramagnetic doublet due to octahedral Fe^{3+} and to a weak doublet due to octahedral Fe^{2+}. Mössbauer parameters are summarized in Table 1. Each doublet has δ values 0.42–0.49 and 1.11–1.28 mms^{-1} due to octahedral Fe^{3+} and octahedral Fe^{2+} ions, respectively. The appearance of FeO_6 octahedra with δ value higher than 0.4 mms^{-1} is evidently consistent with the fact that metal ions form MO_6 octahedra in NASICON-type compounds. After heat treatment, the spectra showed decreasing quadrupole splitting (Δ) values of both Fe^{3+} and Fe^{2+} ions. This means that the local symmetry around the iron atoms was increased as the heat treatment proceeded. It is observed that the relative absorption area (A) for octahedral Fe^{2+} decreased from 27.0 to 14.3 % with an increasing heat treatment time, while octahedral Fe^{3+} exhibited an increasing A value from 73.0 % to 85.7 %. Similar Mössbauer spectra were reported in different NASICON-type compounds containing trivalent iron [19].

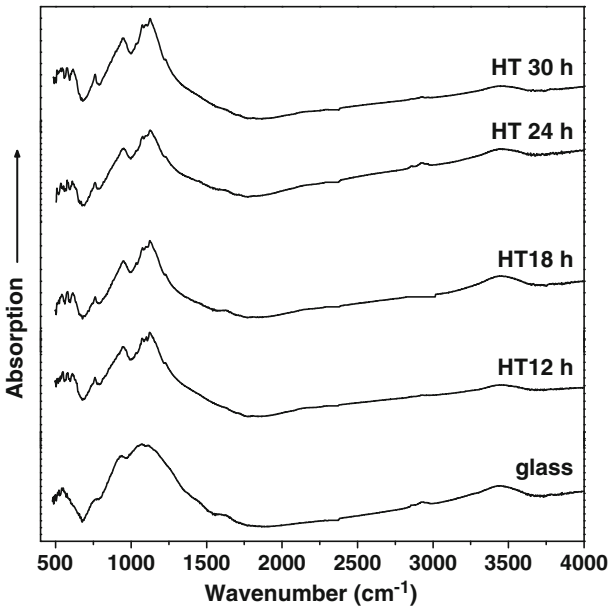

Fig. 4 FTIR absorption spectra of glass and glass-ceramics

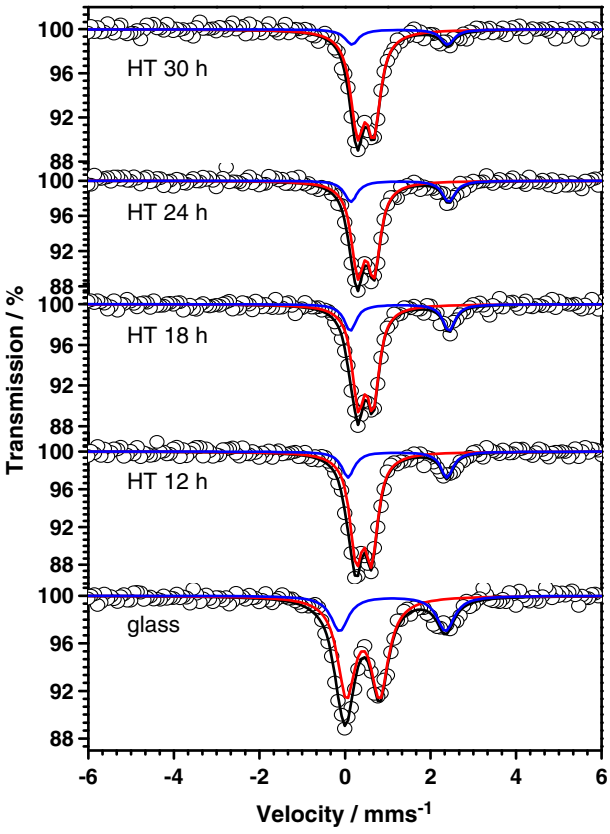

Fig. 5 Mössbauer spectra of glass and glass ceramics measured at room temperature

Table 1 Mössbauer parameters obtained at room temperature before and after heat treatment (HT)

Sample	Fe^{3+}			Fe^{2+}		
	δ (mms^{-1})	Δ (mms^{-1})	A (%)	δ (mms^{-1})	Δ (mms^{-1})	A (%)
Glass	0.42	0.78	73.0	1.11	2.48	27.0
HT for 12 h	0.44	0.36	78.8	1.23	2.31	21.2
HT for 18 h	0.48	0.35	77.2	1.28	2.31	22.8
HT for 24 h	0.49	0.38	79.8	1.28	2.29	20.2
HT for 30 h	0.48	0.38	85.7	1.28	2.24	14.3

3.5 Density

Density of glass and glass ceramics are listed in Table 2. As expected, glass ceramics had higher density than as-quenched glass sample. The gradual increase in the density of glass ceramic will be associated with the rearrangement of the structural units causing more closely-packed structure than in glass [8].

3.6 Impedance spectroscopy analysis

Impedance measurement is a versatile tool that is often used to characterize the response of ionic conductors [20]. Figure 6 shows the complex impedance plots (Cole–Cole plot) of glass and glass ceramic samples measured at 300 K. In the glassy sample, "semicircle" was observed at 300 K, whereas the glass ceramics showed "semicircle and spike" at 300 K. Impedance spectra having spike in low frequency region are due to the surface-related artifacts between the electrode and the sample, being known as an electrode polarization effect. The appearance of low-frequency tail in the case of ionically-blocked electrodes is an indication of the ionic nature of the NASICON-type material [21–24]. The value of bulk resistance R_b was determined from the intersection of the semicircle with the real axis of the impedance Z'.

3.7 Electrical conductivity

Electrical conductivity of the glass and glass ceramics are plotted in Fig. 7. Straight line obtained from the Arrhenius plot yields activation energy (E_{dc}) according to the relationship:

$$\sigma_{dc} = \sigma_o \exp\left(\frac{-E_{dc}}{k_B T}\right) \tag{2}$$

where σ_o is the pre-exponential factor, E_{dc} the activation energy, k_B the Boltzmann constant. Values of E_{dc} for the electrical conduction are summarized in Table 2, from which we can know that σ of 3.70×10^{-6} Sm^{-1} and E_{dc} of 0.42 eV were obtained at 300 K when the glass was heat treated for 24 h at temperature higher than T_c. It is noted that as-quenched glass had smaller σ of 1.16×10^{-9} Sm^{-1} and larger E_{dc} of 0.70 eV at 300 K.

It is noteworthy that the conductivity of glass ceramic, heated for 24 h above T_c, is three orders of magnitude larger than that of as-quenched glass. The enhancement of the conductivity may be attributed to the formation of conducting crystalline phase

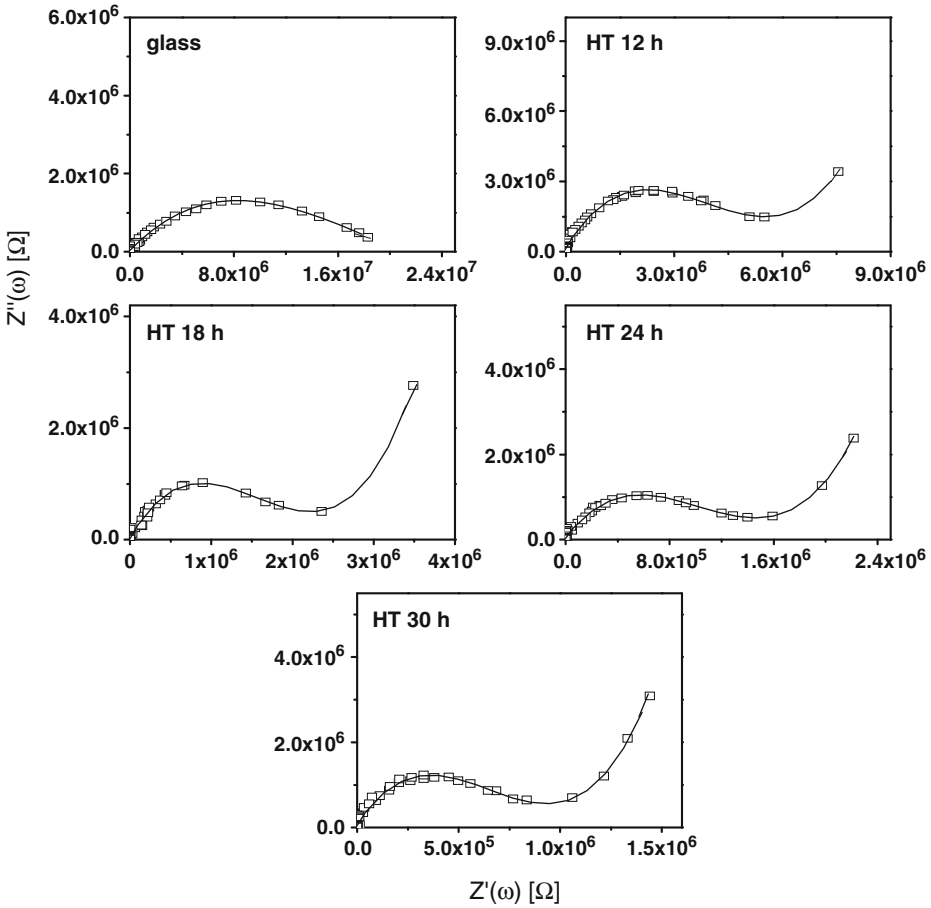

Fig. 6 Cole–Cole plot of glass and glass ceramics measured at 300 K

with NASICON-type structure, together with the percolation effect of the remaining glass matrix. It is generally known that glass ceramic generally consists of crystalline grains or phase precipitated in the glass matrix. If a NASICON-type structure was formed in the crystalline grains, it will provide suitable channels for the migration of Li^+ ions. It is also speculated that glass matrix surrounding the crystalline grains will form a NASICON-like structure [25, 26]. As a result, percolation paths will be created between the grains [25, 26], and the energy barrier for the mobile ions to move in the glass ceramics will become much lower than that in the as-quenched glass, accompanying an enhancement of the ionic conductivity. Probability of the electron conduction due to small polaron hopping from Fe^{2+} to Fe^{3+} ions, if present, will be decreased in the glass ceramic, since the fraction of Fe^{2+} was decreased by the heat treatment, as elucidated in the Mössbauer study. From Table 2, we can understand that the behavior of σ_{dc} is consistent with that of dc conductivity $\sigma(0)$ determined from the complex impedance plots (see Fig. 6).

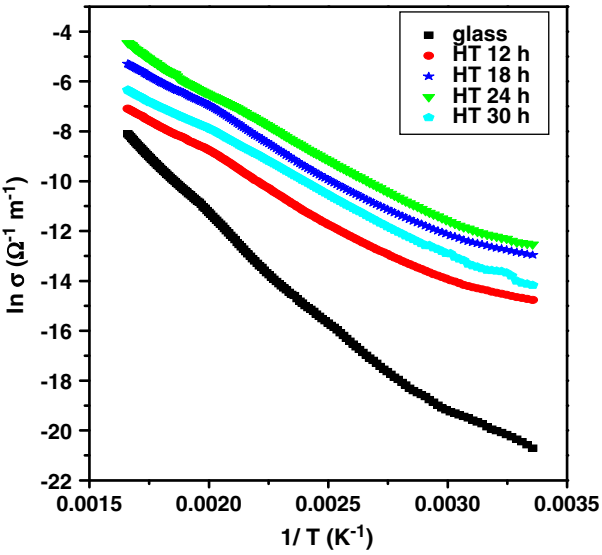

Fig. 7 DC conductivity of glass and glass-ceramics

Table 2 DC conductivities measured at 300 K, activation energy of conduction (E_{dc}) and density of glass and glass ceramics

Sample	From DC conductivity		From AC impedance	Density
	σ_{dc} at 300 K (Sm^{-1})	E_{dc} (eV)	$\sigma(0)$ at 300 K (Sm^{-1})	(gcm^{-3})
Glass	1.16×10^{-9}	0.70	2.13×10^{-6}	3.06
HT for 12 h	4.03×10^{-7}	0.47	1.01×10^{-5}	3.15
HT for 18 h	2.44×10^{-6}	0.45	2.62×10^{-5}	3.19
HT for 24 h	3.70×10^{-6}	0.42	3.48×10^{-5}	3.28
HT for 30 h	7.34×10^{-7}	0.44	5.62×10^{-6}	3.35

4 Conclusion

After heat treatment of $Li_{1.3}Nb_{0.3}Fe_{1.7}(PO_4)_3$ glass, precipitation of NASICON-type $Li_3Fe_2(PO_4)_3$ and $LiFe(P_2O_7)$ of monoclinic structure was confirmed by XRD. Calculated crystallite size exhibited an increasing size from 82 to 124 nm with an increasing heat treatment time. Heat-treated sample at above T_c for 24 h exhibited a highest ionic conductivity at 300 K which was about three orders of magnitude larger than that of as-quenched glass. Mössbauer results at room temperature showed the presence of octahedral Fe^{2+} and Fe^{3+} ions. After the heat treatment, Mössbauer spectra showed that Δ values of both Fe^{3+} and Fe^{2+} were gradually decreased with the increasing heat treatment time. This means that the local symmetry around the iron nucleus was increased as the heat treatment time was prolonged. It was also observed that the relative absorption area (A) of Fe^{2+} showed a gradual decrease after the heat treatment, while Fe^{3+} showed an increase in A. Density of heat-treated samples was gradually increased from 3.06 to 3.35 gcm^{-3} with an increasing heat treatment time. Impedance study showed a low frequency tail in heat-treated samples

due to the precipitation of ionic NASICON-type nanocrystals, which increased the DC conductivity.

References

1. Robertson, A.D., West, A.R., Ritchie, A.G.: J. Solid State Ionics. **104**, 1 (1997)
2. Woodcock, D.A., Lightfoot, Ph., Ritter, C.: J. Chem. Commun. **19**, 107 (1998)
3. Hagman, L.O., Kierkegaard, P.: Acta Chem. Scand. **22**, 1822 (1968)
4. Goodenough, J.B., Hong, H.P.Y.: Mater. Res. Bull. **11**, 203 (1976)
5. Sudreau, F., Petit, D., Boilot, J.P.: J. Solid State Chem. **83**, 78 (1989)
6. Hamdoune, S., Gondran, M., Tran Qui, D.: Mater. Res. Bull. **21**, 237 (1986)
7. Gorzkowska1, I., Jozwiak, P., Garbarczyk, J.E., Wasiucionek, M., Julien, C.M.: J. Therm. Anal. Calorim. **93**, 759 (2008)
8. Duhan, S., Sanghi, S., Agarwal, A., Sheoran, A., Rani, S.: Phys. B **404**, 1648 (2009)
9. Williamson, G.K., Hall, W.H.: Acta Metal. **1**, 22 (1953)
10. Nakaumoto, K.: Infrared and Raman Spectra of Inorganic and Coordination Compounds: Part A. Theory and Applications in Inorganic Chemistry. Wiley, New York (1997)
11. Dayanand, C., Bhikshamaiah, G., Jayatyagareju, V., Salagram, M., Krishnamurthy, A.S.R.: J. Mater. Sci. **31**, 1945 (1996)
12. Hudgens, J.J., Martin, S.W.: J. Am. Ceram. Soc. **76**, 1691 (1994)
13. Mazali, I.O., Barbosa, L.C., Alves, O.L.: J. Mater. Sci. **39**(6), 1987 (2004)
14. Nyquist R.A., Putzig C.L., Leugers M.A.: Infrared and Raman Spectral Atlas of Inorganic Compounds and Organic Salts: Raman Spectra. Academic Press, San Diego (1997)
15. Selvaraj, U., Rao, K.J.: J. Non-Cryst. Solids **72**, 315 (1985)
16. Corbidge, D.C., Lowe, E.J.: J. Chem. Soc., Part I 493 (1954)
17. Miller, F.A., Wilkins, C.H.: Anal. Chem. **24**, 1253 (1952)
18. Hayri, E.A., Greenblatt, M.: J. Non-Cryst. Solids **94**(3), 387–401 (1987)
19. Ignaszak, A., Komornicki, S., Pasierb, P.: Ceram. Internat. **35**, 2531 (2009)
20. Macdonald, J.R.: Impedance Spectroscopy Emphasizing Solid Materials and Systems. Wiley, New York (1987)
21. Nairn, K.M., Forsytha, M., Greville, M., MacFarlane, D.R., Smith, M.E.: Solid State Ionics. **86–88**, 397 (1996)
22. Forsyth, M., Wong, S., Nairn, K.M., Best, A.S., Newman, P.J., MacFarlane, D.R.: Solid State Ionics. **124**, 213 (1999)
23. Irvine, J.T.S., Sinclair, D.C., West, A.R.: Adv. Mater. **2**, 132 (1990)
24. Thangadurai, V., Huggins, R.A., Weppner, W.: J. Power Sources. **108**, 64 (2002)
25. Chowdari, B.V.R., Subba Rao, G.V., Lee, G.Y.H.: Solid State Ionics. **136–137**, 1067 (2000)
26. Zhang, Q., Wen, Z., Liu, Y., Song, S., Wu, X.: J. Alloy. Comp. **479**, 494 (2009)